Farnesiferol C enhances the effects of chemotherapy and ionising radiation in human melanoma cells via targeting topoisomerase II alpha

Negin Moosavinejad , Zahra Nasiri Sarvi , Hamid Gholamhosseinian , Mehrdad Iranshahi & Fatemeh B. Rassouli

View supplementary material

Published online: 30 Sep 2025.

Submit your article to this journal

View related articles

View Crossmark data

Taylor & Francis
Taylor & Francis Group

RESEARCH ARTICLE

OPEN ACCESS

Check for updates

Farnesiferol C enhances the effects of chemotherapy and ionising radiation in human melanoma cells via targeting topoisomerase II alpha

Negin Moosavinejad[a,b], Zahra Nasiri Sarvi[a,b], Hamid Gholamhosseinian[c], Mehrdad Iranshahi[d] and Fatemeh B. Rassouli[a,b]

[a]Novel Diagnostics and Therapeutics Research Group, Institute of Biotechnology, Ferdowsi University of Mashhad, Mashhad, Iran; [b]Department of Biology, Faculty of Science, Ferdowsi University of Mashhad, Mashhad, Iran; [c]Department of Medical Physics, Faculty of Medicine, Mashhad University of Medical Sciences, Mashhad, Iran; [d]Biotechnology Research Center, Pharmaceutical Technology Institute, Mashhad University of Medical Sciences, Mashhad, Iran

ABSTRACT

This study evaluated Farnesiferol C (FC), a natural coumarin, as a potential topoisomerase IIα (TOP2A) inhibitor to enhance chemotherapy and ionising radiation (IR) efficacy in melanoma cells. Key targets were identified, followed by enrichment and gene expression analyses, and molecular docking and dynamics simulations. Upon extraction of FC from *Ferula szowitsiana*, cell treatment with FC, alone or combined with IR or temozolomide (TMZ), was performed, and viability and apoptosis were assessed. TOP2A emerged as a hub target, showing elevated expression in melanoma and a negative correlation with patient survival. Simulations demonstrated stable binding of FC at the ATP-binding site of TOP2A. Experimental data revealed selective cytotoxicity of FC on A375 melanoma cells (IC$_{50}$: 76.9 μM, SI: 4.97), sparing normal fibroblasts. Combination treatments with IR or TMZ further increased cytotoxicity and apoptosis. These findings suggest FC as a promising TOP2A inhibitor that potentiates the DNA damage effects of chemoradiotherapy in melanoma.

1. Introduction

Melanoma represents the most aggressive and lethal subtype of skin cancer[1]. Early-stage melanoma is primarily managed through surgical excision of the tumour; however, treatment of advanced-stage disease remains challenging and multifaceted[2]. Current therapeutic modalities include chemotherapy with agents such as temozolomide (TMZ) and dacarbazine, radiotherapy, immunotherapy, and targeted therapies[3–6]. Despite their clinical utility, these approaches are often hindered by inherent or acquired resistance, off-target cytotoxicity affecting normal tissues, and immune-related adverse events—including severe dermatologic toxicities—that can necessitate treatment discontinuation and adversely impact patient prognosis[7–9]. Emerging modalities such as radiodynamic therapy, ultrasound technology, and nanotechnology have contributed to enhancing the efficacy of conventional treatments[10–13]. Nonetheless, considerable interest persists in the development of natural compounds as adjuvants to sensitise malignant cells to chemotherapy and ionising radiation (IR) by modulating key pathways involved in therapeutic resistance mechanisms.

DNA topoisomerases orchestrate the modulation of DNA topology by inducing transient single- or double-stranded breaks, thereby relieving torsional stress during replication and transcription processes[14]. Two isoforms of type II topoisomerase include topo IIα (TOP2A), which is predominantly expressed in proliferating cells, and topo IIβ (TOP2B), which is ubiquitously present across both dividing and quiescent cell populations[15,16]. TOP2A functions as a homodimeric enzyme composed of four principal domains,

including the N-gate harbouring an ATP-binding motif characteristic of the GHKL ATPase family, the DNA gate, the C-gate, and the C-terminal domain, with catalytic activity reliant upon Mg^{2+} ions and ATP hydrolysis[17,18]. TOP2 inhibitors are broadly classified into catalytic inhibitors, which obstruct DNA binding, cleavage, or ATPase activity without inducing DNA strand breaks, and TOP2 poisons, which stabilise the cleavage complex, thereby enhancing DNA damage[19]. By disrupting topoisomerase function, these agents induce DNA lesions culminating in cell death, underscoring the longstanding therapeutic relevance of TOP2 as an oncology drug target[20].

Farnesiferol C (FC), a sesquiterpene coumarin predominantly isolated from the roots of Ferula species, is a polycyclic aromatic compound characterised by a 1-benzopyran core and a ketone functional group at the C2 position[21,22]. FC demonstrates a broad spectrum of pharmacological properties, encompassing antiviral, anti-inflammatory, and neuroprotective activities[23–27]. Moreover, FC has exhibited notable cytotoxic effects against various cancer cell lines, both as a monotherapy and in synergy with conventional chemotherapeutics. For example, FC induced apoptosis and significantly inhibited viability in human breast, cervical, and oesophageal carcinoma cells[28]. In chronic myelogenous leukaemia models, FC treatment resulted in G_1 phase cell cycle arrest, cleavage of PARP and caspases 9 and 3, downregulation of cyclins D1, E, and B1, and potentiated the apoptotic efficacy of Imatinib[26]. Additionally, FC promoted apoptosis and G_1 arrest in non-small cell lung cancer cells through suppression of anti-apoptotic proteins such as BCL-2, BCL-xL, Survivin, and procaspase-3, and exhibited synergistic effects with Puromycin and Doxorubicin[29]. Furthermore, FC enhanced the cytotoxicity of Doxorubicin in breast carcinoma cells by inhibiting P-glycoprotein-mediated drug efflux, thereby reversing multidrug resistance[30]. Despite these promising anticancer properties, the effects of FC—both alone and in combination with other therapies—on melanoma cells remain unexplored.

To address this critical knowledge gap, the present study constitutes a novel investigation into the potential of FC as a TOP2A inhibitor capable of augmenting the DNA-damaging efficacy of radiotherapy and an alkylating agent in human melanoma cells. Initially, key molecular targets were identified, and enrichment and gene expression analyses were performed. Subsequently, molecular docking and dynamic simulations were employed to characterise the binding interactions of FC within the ATP-binding site of TOP2A. Experimentally, FC was isolated from Ferula szowitsiana, and its effects on the viability of human melanoma cells and normal fibroblasts were evaluated following treatments with FC alone as well as in combination with IR or TMZ. Additionally, apoptosis induction was quantitatively assessed via flow cytometry to elucidate the mechanistic impact of FC.

2. Methods

2.1. Computational analyses

2.1.1. Target prediction, interaction and enrichment analyses

To identify genes associated with skin cutaneous melanoma (SKCM), the Open Targets platform (https://platform.opentargets.org/) was employed, which integrates diverse datasets to systematically prioritise disease-related genes[31]. Complementarily, genes significantly overexpressed in SKCM were extracted from GEPIA2 (http://gepia2.cancer-pku.cn/#index) using an ANOVA-based differential expression analysis, comparing tumour RNA-seq data from The Cancer Genome Atlas (TCGA) against paired normal tissue from the Genotype-Tissue Expression (GTEx) project, with a threshold of Log2 fold change (FC) > 1.

Simultaneously, potential molecular targets corresponding to FC were predicted via the SwissTargetPrediction tool (http://swisstargetprediction.ch/)[32]. The input utilised was the SMILES representation (C/C(=C\COC1=CC2=C(C=C1)C=CC(=O)O2)/CC[C@H]3[C@@]4(CCC@HO4)C) retrieved from PubChem (https://pubchem.ncbi.nlm.nih.gov/). Overlapping genes between these datasets were identified through Venn diagram analysis to focus on shared targets.

For elucidation of the protein-protein interaction (PPI) network among common genes, the STRING database (https://string-db.org/) was utilised, applying a stringent confidence score cut-off of ≥ 0.7 to ensure high-quality interactions[33]. The resultant PPI network was subsequently visualised and interrogated using Cytoscape (v3.10.3). To pinpoint critical hub genes within this network, the CytoHubba

plugin was employed, leveraging clustering coefficient metrics to rank nodes by the Density of Maximum Neighbourhood Component (DMNC) method.

Finally, functional enrichment and characterisation of the prioritised gene set were performed using Gene Ontology (GO) analysis via the TNMplot platform, incorporating adjusted *p* values to ensure robust statistical validation of enriched biological processes and molecular functions[34]. This multi-tiered integrative approach provides a comprehensive framework for unveiling key molecular players in SKCM pathogenesis.

2.1.2. Validating the expression of TOP2A and its clinical significance in melanoma

The expression validation of *TOP2A* and its clinical relevance in melanoma was conducted through a multi-database integrative analysis. Initially, differential expression of *TOP2A* in SKCM tissue (*n* = 461) relative to normal tissue (*n* = 558) was examined using the GEPIA2[35]. *TOP2A* expression levels were further evaluated in an independent cohort comprising SKCM samples (*n* = 103) and normal tissues from non-cancerous individuals (*n* = 47) using RNA-seq data retrieved through the TNMplot.

To elucidate the prognostic impact of *TOP2A* expression, Kaplan–Meier survival analyses were conducted to compare overall survival between patients stratified into "high" and "low" expression groups. Statistical significance of survival differences was determined by the log-rank test within the GEPIA2 framework.

To complement these findings at the cellular level, microarray data from the Gene Expression Omnibus (GEO) were analysed. Dataset GSE86373 was selected to assess *TOP2A* expression in the A375 melanoma cell line relative to primary human epidermal melanocytes. Differential expression analysis was performed using the GEO2R tool, where statistical significance was determined with adjusted *p* values computed via the "ggplot2" package in R software, applying stringent criteria of $p < 0.05$ and a Log2 FC > 0.5.

2.1.3. Molecular docking

Molecular docking was performed to elucidate the interaction between FC and TOP2A. The high-resolution crystal structure of human TOP2A (PDB ID: 1ZXM, 1.87 Å) was retrieved from the RCSB Protein Data Bank (https://www.rcsb.org/). The three-dimensional SDF format of FC (ID: 15559239) and Etoposide (ID: 36462), a well-characterised TOP2A inhibitor serving as a positive control, were obtained from the PubChem (https://pubchem.ncbi.nlm.nih.gov/).

Protein preparation was executed using the Protoss tool to optimise protonation states and refine the hydrogen bond network, ensuring an accurate molecular environment for docking. Docking was conducted on the Proteins Plus platform (https://proteins.plus/) utilising the JAMDA algorithm with a site radius constrained to 6.5 Å to focus the search on the active binding pocket[36]. Post-docking, the resultant protein-ligand complexes were visualised and scrutinised with PoseEdit, generating both 2D and 3D interaction diagrams[36–38]. The distance between FC and the docked enzyme was calculated and visualised using PyMOL (v 3.0.3).

2.1.4. Molecular dynamics simulations

To assess the conformational flexibility and binding stability of the FC–TOP2A complex, molecular dynamics simulations were performed. These simulations utilised GROMACS version 2023 equipped with the CHARMM36 all-atom force field. To facilitate the preparation process—which included merging topologies, solvation, energy minimisation, and equilibration steps—a custom Bash script was employed. The system was solvated using the CHARMM-adapted TIP3P water model and neutralised by adding Na$^+$ and Cl$^-$ ions. Energy minimisation proceeded until the maximum force on any atom dropped below 10.0 kJ/mol. Equilibration proceeded under constant volume and temperature (NVT), followed by constant pressure and temperature (NPT), with both phases maintained at 310 K and 1 bar using Parrinello-Rahman coupling. Production runs spanned 100 ns, applying the leapfrog integrator with a 2 fs timestep. Analysis of simulation trajectories encompassed structural stability assessed by root mean square deviation (RMSD), residue-level flexibility via root mean square fluctuation (RMSF), compactness through radius of gyration (Rg), solvent exposure evaluated by solvent-accessible surface

area (SASA), and evaluation of non-bonded interactions via Coulombic and Lennard-Jones potential energy calculations. Data visualisation was performed using the ggplot2 package in R.

2.2. In vitro studies

2.2.1. Extraction of FC

For extraction of FC, *Ferula szowitsiana* was collected from the mountains of Golestan forest with the necessary permissions from local authorities. The plant material was formally identified by a botanical expert at the Faculty of Pharmacy, Mashhad University of Medical Sciences (MUMS), to ensure the accuracy of the species. A voucher specimen of the roots (No. M1001) was deposited at the Department of Pharmacognosy and Biotechnology, Faculty of Pharmacy, MUMS, Iran. The extraction of FC was performed as previously described[39]. Briefly, roots of *Ferula szowitsiana* were air-dried, ground into powder, and macerated in acetone (Merck) at room temperature. After filtration, the extract was concentrated under reduced pressure to obtain a brownish residue, which was subjected to silica gel column chromatography using a petroleum ether/acetone gradient. Fractions were analysed by thin-layer chromatography (TLC) on silica gel plates with a petroleum ether/ethyl acetate mobile phase. Final purification of FC was achieved by preparative TLC, and its structure was confirmed by ^{1}H- and ^{13}C-NMR spectroscopy (Figure 1).

2.2.2. Single and combinatorial treatments of cells

Human melanoma cells (A375 cell line) and human normal fibroblasts (HFF-3 cell line), procured from the Pasteur Institute (Tehran, Iran), were cultured in Dulbecco's Modified Eagle's Medium—high glucose (Capricorn) supplemented with 10% foetal bovine serum (Neofroxx). Cells were maintained under standard conditions at 37°C in a humidified atmosphere with 5% CO_2 and subcultured upon reaching confluency using 0.25% trypsin-1mM EDTA (Betacell).

Stock solutions of FC (MW: 382.5g/mol) were prepared in dimethyl sulfoxide (DMSO). Final concentrations of 25, 50, and 100μM were freshly prepared in complete medium prior to use, and a solvent control containing 0.3% DMSO was included. Cells were seeded in 96-well plates (4,000 cells/well) and treated with FC for 72 and 120h, after which cell viability was assessed and IC_{50} values were determined.

For combined treatment with IR, cells were pre-treated with 25 and 50μM FC for 48h, then exposed to IR doses of 4, 6, and 8Gy using the Elekta Compact™ linear accelerator (Crawley). These IR doses were selected based on established radiation oncology protocols, balancing effective induction of cellular damage and evaluation of potential radiosensitizing effects. After 72h recovery, cell viability was assessed. Controls included untreated cells and cells pre-treated with 0.3% DMSO exposed to the corresponding IR doses.
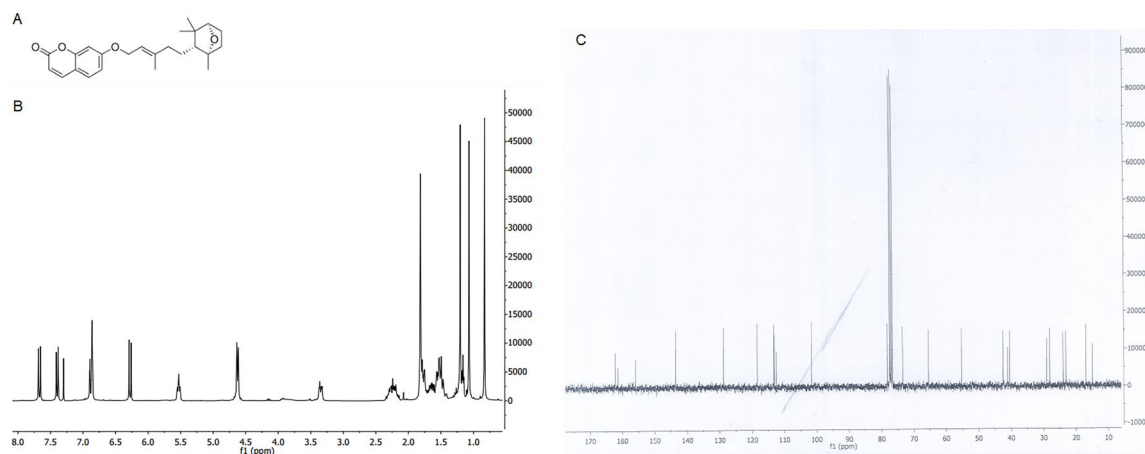

Figure 1. Chemical structure of FC (A) and its corresponding proton (^{1}H) NMR spectrum (B) and carbon-13 (^{13}C) NMR spectrum (C).

For combinatorial treatment with TMZ, the viability of cells was first determined by treating cells with 100, 200, 400, and 600 μM TMZ (Merck). Subsequently, A375 cells were treated with combinations of 25 and 50 μM FC plus 200 and 400 μM TMZ for 72 h, followed by viability assessment. Controls included untreated cells and cells treated with 0.3% DMSO combined with corresponding TMZ concentrations.

2.2.3. Cell viability assay

Cell viability after single and combination treatments was evaluated using the resazurin assay. Briefly, resazurin solution (0.1 mg/ml, Sigma) was added to the cells at the end of each time point, followed by 3 h incubation at 37 °C. Absorbance was then measured at 600 nm using a microplate reader (Epoch). Cell viability (%) was calculated as $(100 - (AT - AU)/(AB - AU)) \times 100$, where AT, AU, and AB represent the absorbance values of treated cells, untreated cells, and blank control, respectively.

2.2.4. Apoptosis assay

To assess apoptosis, A375 cells treated with 50 μM FC, 400 μM TMZ, their combination, and DMSO control were harvested after 72 h, washed with PBS, and resuspended in binding buffer containing annexin V-FITC and propidium iodide (PI, Sigma). Flow cytometric data were collected using FL1-H and FL2-H channels (BD FACSCalibur), enabling discrimination of viable cells (negative for both annexin V and PI), necrotic cells (PI-positive only), and early and late apoptotic cells (annexin V-positive).

2.2.5. Statistical analyses

Data were analysed statistically using one-way ANOVA for multiple comparisons with GraphPad Prism software (v 10.4.1). The results are presented as mean ± standard deviation (SD), and statistical significance was determined for p values < 0.05, 0.01, 0.001, and 0.0001.

3. Results

Target screening identified 3,789 genes associated with SKCM, 2,541 genes overexpressed in SKCM, and 205 predicted targets of FC. Venn analysis revealed 24 overlapping protein-coding genes (Figure 2A), which were used to construct the PPI network via STRING. These genes included *MET, CDK1, MMP1, CCNB2, CDK2, KIF11, SOAT1, TOP2A, ACSL3, AURKA, AURKB, CTSB, ITGB1, FCGR3A, CDK4, PIK3CD, STAT1, ADORA3, TGM2, CTSS, ADAM10, CTSD, CTSL,* and *CDK5* (Figure 2B). The resulting network was then visualised in Cytoscape (v3.10.3), comprised 22 nodes and 61 edges. Using the CytoHubba plugin with the DMNC ranking method, *AURKB, TOP2A, KIF11, CCNB2,* and *AURKA* were identified as the five top hub genes (Figure 2C).
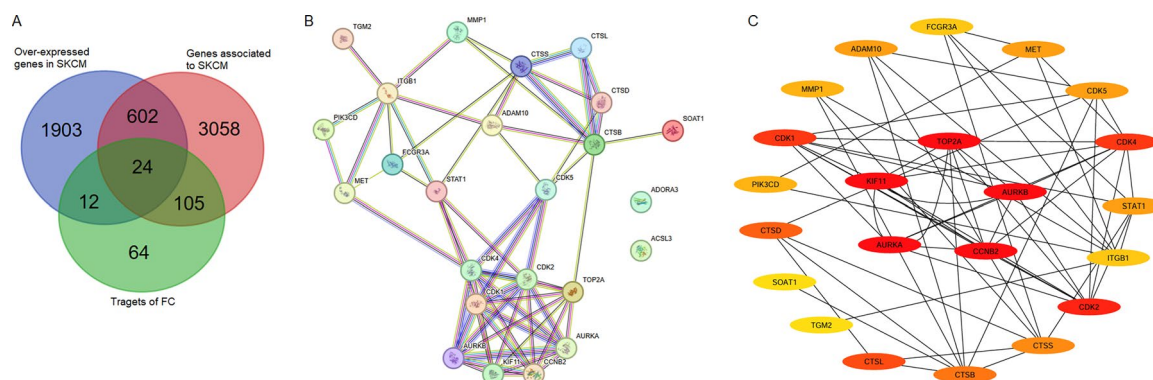
Figure 2. Identification of shared targets and PPI network for hub genes. Venn diagram showing the overlap among overexpressed genes in SKCM, SKCM-associated genes, and protein targets of FC (A). STRING-based interactome mapping of the shared targets, illustrating their functional associations (B). Cytoscape visualisation of the PPI network comprising 22 nodes and 61 edges, highlighting five top hub genes (C). Node colours represent expression levels, ranging from significantly high (red) to low (yellow).

Enrichment analysis of the identified hub targets revealed significant biological process terms, including modification, phosphorylation, apoptosis, and mitotic cell cycle phase transition, all with adjusted $p \leq 0.05$, underscoring their involvement in cell proliferation and apoptotic regulation (Figure 3A). Within the molecular function category, terms such as endopeptidase activity, serine/threonine kinase activity, and cyclin-dependent protein kinase activity were significantly enriched ($p \leq 0.05$), highlighting the enzymatic and kinase-related roles of the hub genes (Figure 3B).

To evaluate the clinical significance of TOP2A in SKCM, multi-database analyses of tissue samples were conducted. Expression analysis via GEPIA2 demonstrated a significant ($p < 0.01$) upregulation of *TOP2A* in tumour tissues compared to normal controls (Figure 4A). Concordantly, analysis using TNMplot, with the Mann–Whitney test, revealed markedly ($p = 1.07e-33$) elevated *TOP2A* expression in SKCM samples (Figure 4B). The Kaplan–Meier survival analysis, spanning a follow-up period of 300 months, stratified patients into high ($n = 229$) and low ($n = 229$) *TOP2A* expression groups (Figure 4C). Patients with high *TOP2A* expression (red dashed line) exhibited poorer survival outcomes, with overall survival declining to approximately 20% at 300 months, whereas the low-expression group (blue dashed line) showed a more gradual decrease, maintaining survival above 40% at the same time point. The log-rank test yielded a marginally non-significant difference between groups ($p = 0.073$), with a hazard ratio of 1.3, indicating a trend towards reduced survival associated with elevated *TOP2A* expression in SKCM. Further, differential expression analysis of the GSE86373 dataset was performed in R to compare *TOP2A* levels in A375 melanoma cells versus normal human epidermal melanocytes. As illustrated in the volcano plot (Figure 4D), *TOP2A* expression was significantly ($p < 0.05$) upregulated in A375 cells relative to controls.

Given the pivotal role of TOP2A within the PPI network and its critical functional relevance, molecular docking was performed to evaluate and compare the binding affinity of FC with that of the established TOP2A inhibitor, Etoposide. As illustrated in Figure 5, FC demonstrated a favourable binding profile to TOP2A, with a JAMDA docking score of −2.56791. This interaction was characterised by multiple stabilising contacts, including hydrogen bonds and hydrophobic interactions with key residues Ser148, Ser149, Arg162, and Lys378, suggesting strong and specific engagement with the ATP-binding site of the enzyme. Figure S1 details the distances between FC atoms and critical TOP2A residues: 2.2 Å between Ser148 (H from OH of side chain and O from FC), 2.1 Å and 2.5 Å involving Ser149 (H from backbone NH and OH of side chain respectively with O from FC), 2.6 Å for Arg162 (H from backbone NH and O from FC), and 2.0 Å for Lys378 (H from NH3+ side chain and O from FC). Compared to FC, Etoposide exhibited a slightly lower binding affinity, reflected by a JAMDA score of −2.05754, forming hydrogen bonds predominantly with Ser148 and Ser149 and hydrophobic contacts involving Pro126, Val137, Ile141, and Ser149. These findings underscore the potential of FC as a TOP2A-targeting agent, with its distinct interaction pattern and superior docking score indicating a robust binding capacity.
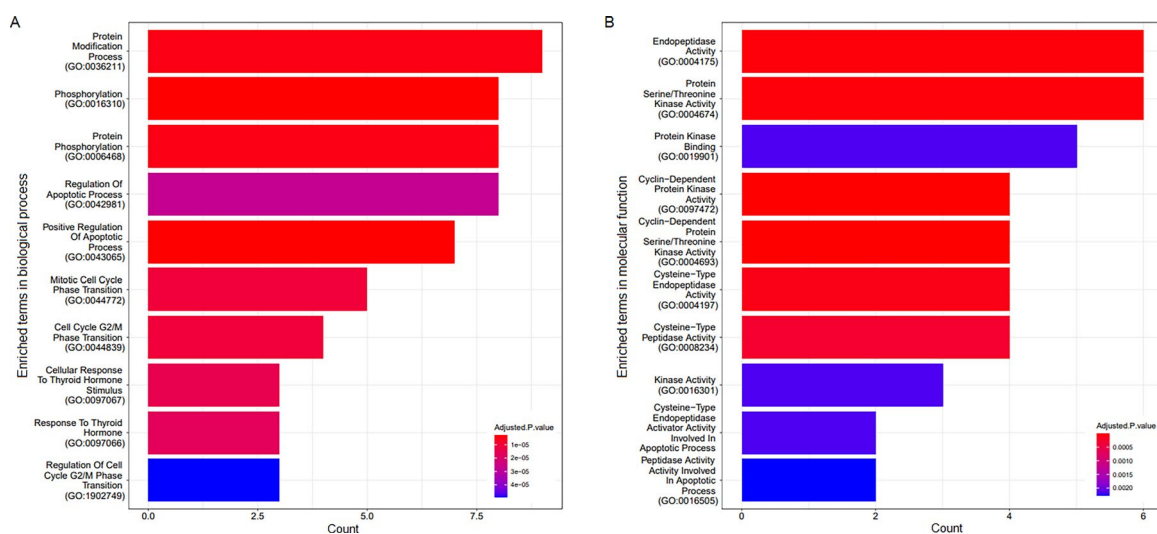

Figure 3. Gene set enrichment analyses. Gene ontology enrichment analyses identified significant terms in biological process (A) and molecular function (B).
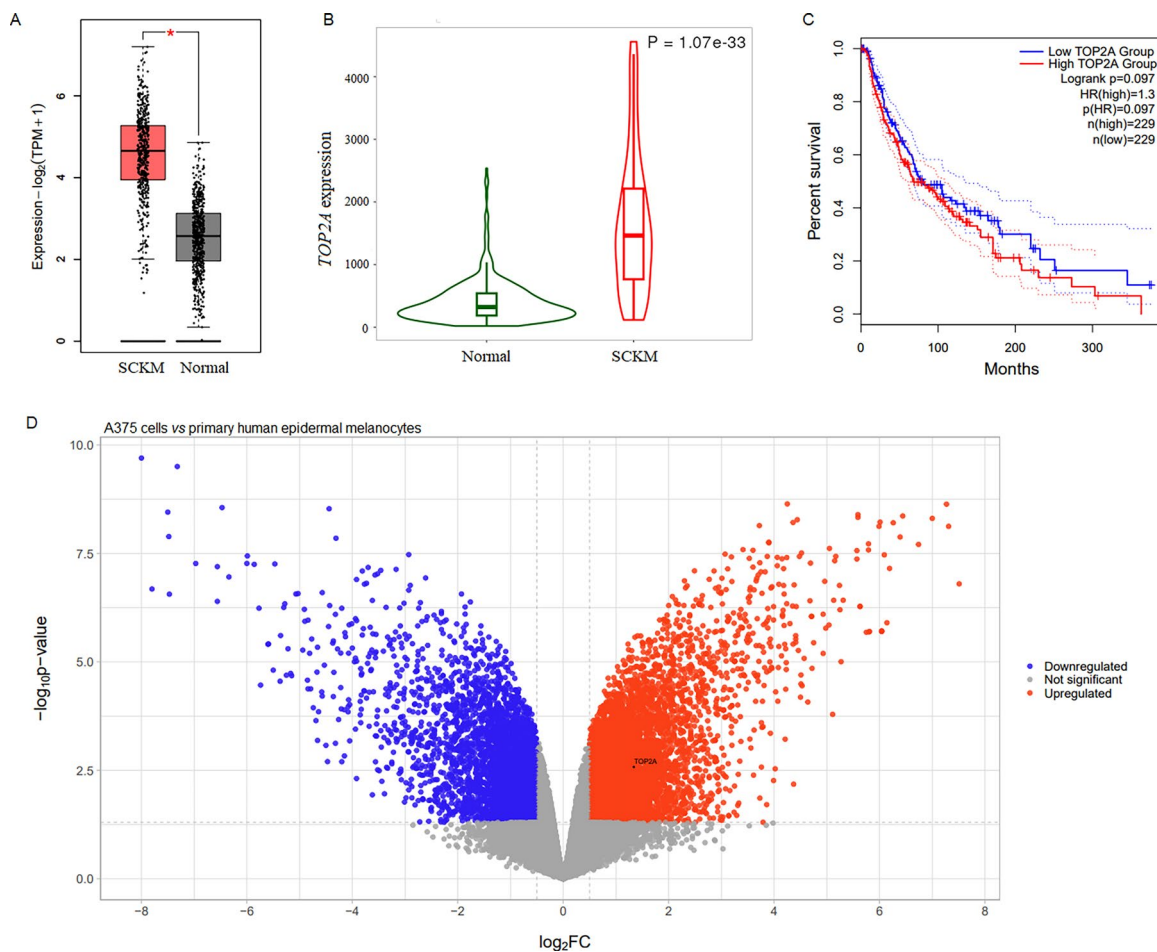
Figure 4. Validating the expression of *TOP2A* in melanoma. Differential expression of *TOP2A* in SKCM tissue ($n=461$) relative to normal tissue ($n=558$) in GEPIA2 (A). *TOP2A* expression in an independent cohort comprising SKCM samples ($n=103$) and normal tissues from non-cancerous individuals ($n=47$) in TNMplot (B). Kaplan-Meier overall survival curves of SKCM patients (C) stratified by *TOP2A* expression level: low ($n=229$) and high ($n=229$). Volcano plot from differential expression analysis of GSE86373 showing significant upregulation of *TOP2A* in A375 cells relative to epidermal melano-cytes (D).
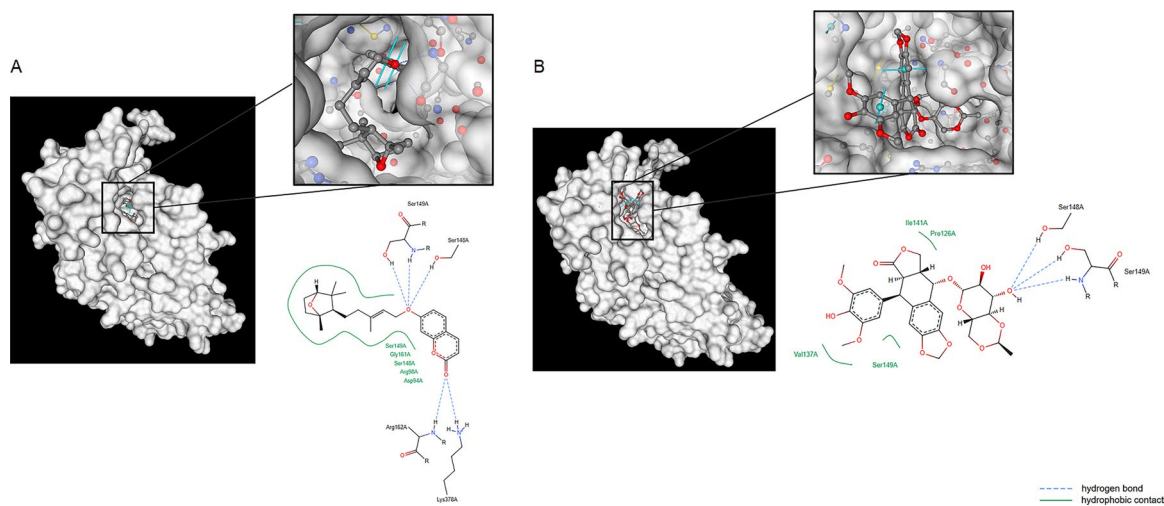

Figure 5. Molecular docking diagrams of ligands binding to TOP2A. The 3D and 2D interaction illustrations of FC (A) and Etoposide (B) with the ATP-binding site of TOP2A. Images were generated using PoseEdit on the ProteinsPlus web server.

The interaction dynamics between FC and TOP2A were also examined to assess the stability and structural integrity. The mean RMSD values for the FC-TOP2A complex were 3.945 Å, indicating stable binding accompanied by some rotational movement within the TOP2A catalytic domain (Figure 6A). The RMSF analysis showed that most residues of TOP2A exhibited fluctuations below 1.587 nm when bound to FC, suggesting limited conformational change (Figure 6B). The Rg remained constant during the simulation, demonstrating maintenance of a compact structural arrangement (Figure 6C). Assessment of SASA resulted in an average value of 200.05 nm² for the complex, reflecting significant exposure of both hydrophilic and hydrophobic residues that could promote ligand binding (Figure 6D). Furthermore, analysis of interaction energies by Coulombic and Lennard-Jones potentials demonstrated consistent and favourable binding between TOP2A and FC throughout the simulation, confirming a strong affinity (Figures 6E-F).

Building on computational analyses indicating FC targets TOP2A, we evaluated its effects on the toxicity of IR and chemotherapy. Initially, FC was extracted, and its half-maximal inhibitory concentration (IC_{50})
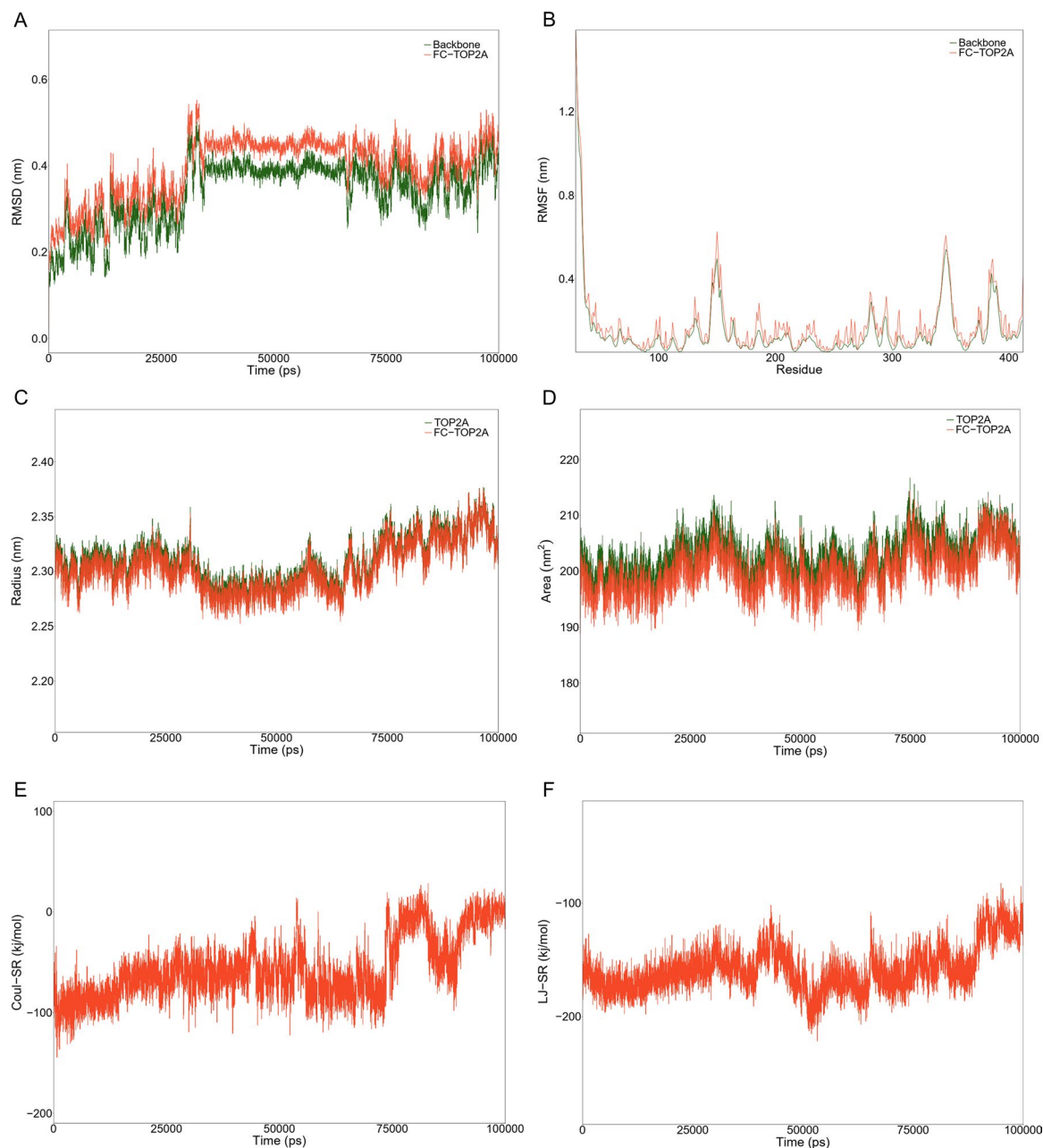

Figure 6. Stable interaction of FC with the ATP-binding site of TOP2A. Plots generated from 100 ns molecular dynamics simulations, demonstrating structural and energetic properties of the FC-TOP2A complex: RMSD (A), RMSF (B), Rg (C), and SASA (D), short-range Coulombic potential (E) and short-range Lennard-Jones potential (F).

and selectivity index (SI) were determined. In A375 cells, the IC_{50} values were 81.26 μM at 72 h and 76.99 μM at 120 h. For HFF-3 normal fibroblasts, the IC_{50} values were significantly higher, at 403.87 μM and 309.13 μM at 72 and 120 h, respectively. The resulting selectivity index (SI) values were 4.97 and 4.01 at 72 and 120 h, respectively, demonstrating selective cytotoxicity of FC towards melanoma cells.

To evaluate the combined effects of FC and IR, A375 and HFF-3 cells were pre-treated with 25 and 50 μM FC for 48 h, followed by IR exposure and 72 h recovery. As shown in Figure 7(A), the viability of A375 cells pre-treated with DMSO and then exposed to 4, 6, and 8 Gy IR was 95.06%, 95.04%, and 93.17%, respectively. After 48 h pre-treatment with 25 μM FC following 4, 6, and 8 Gy IR and recovery, viability was 88.57% ($p < 0.05$), 85.74% ($p < 0.05$), and 83.92% ($p < 0.01$), respectively. With 50 μM FC, IR toxicity increased significantly compared to the DMSO control, reducing viability to 70.37% ($p < 0.001$), 67.14% ($p < 0.001$), and 57.84% ($p < 0.0001$), respectively. Assessment of HFF-3 cells after 120 h treatment with 25 and 50 μM FC, alone or combined with 6 Gy IR, did not show considerable cytotoxicity (Figure 7B).

The viability of A375 cells was also assessed after treatment with 25 and 50 μM FC combined with 200 and 400 μM TMZ for 72 h. As shown in Figure 7(C), viability was 87.67% and 65.08% for 25 and 50 μM FC alone, respectively. Notably, combination treatment with 50 μM FC and 400 μM TMZ significantly ($p < 0.0001$) reduced cell viability to 58.60%, compared to 75.54% for the combined DMSO and TMZ control.

To identify the type of cell death observed in resazurin assay, annexin V-PI staining was performed. As shown in Figure 8(A), the DMSO control exhibited 83.7% viable cells and 14.4% late apoptotic cells. Treatment with 50 μM FC showed 68.3% viability, with 3.59% early and 24.4% late apoptosis. With 400 μM TMZ, 77.1% of cells were viable and 21.1% were late apoptotic. Combined treatment with 50 μM FC and 400 μM TMZ reduced viability to 58.8%, with 2.16% early and 37% late apoptotic cells. Morphological
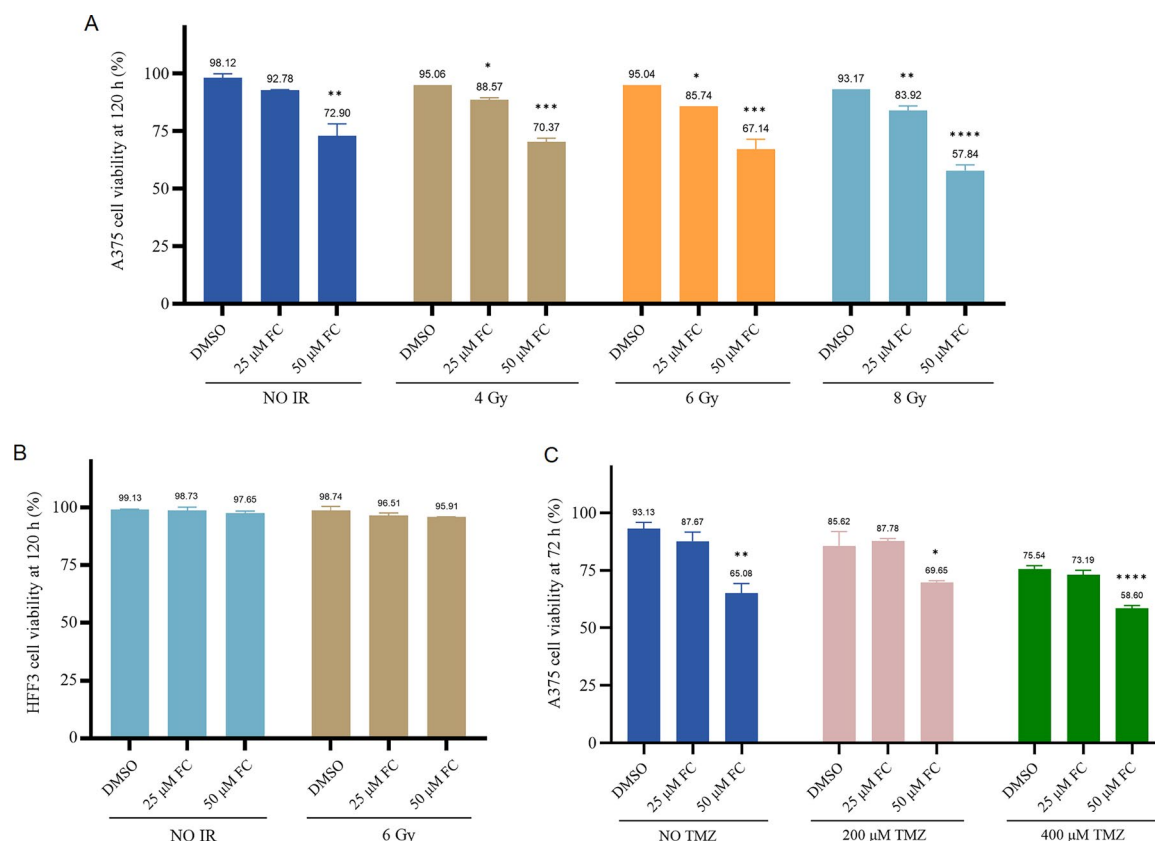
Figure 7. Viability of cells treated with FC alone and combined with IR or TMZ. After 48 h pre-treatment with 25 and 50 μM FC, A375 cells were exposed to 4, 6, and 8 Gy IR, followed by 72 h recovery before viability measurement (A). HFF-3 cells were treated with 25 and 50 μM FC, then exposed to 6 Gy IR and allowed 72 h recovery before viability assessment (B). A375 cells were treated with 25 and 50 μM FC alone or combined with 200 and 400 μM TMZ for 72 h (C). Results are presented as mean ± SD, with statistical significance compared to corresponding DMSO controls indicated as *$p < 0.05$, **$p < 0.01$, ***$p < 0.001$, and ****$p < 0.0001$.

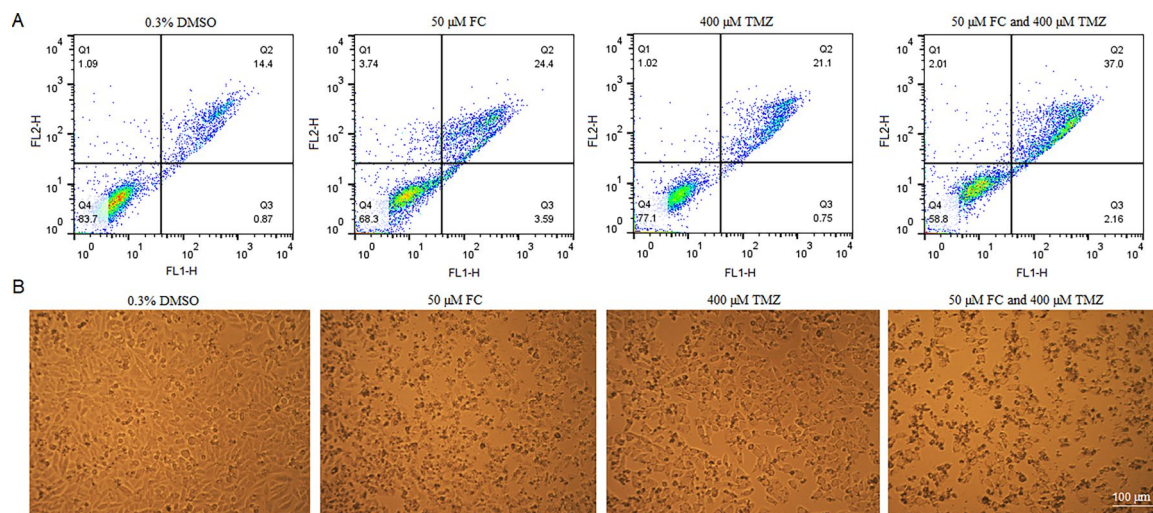**Figure 8.** Flow cytometry analyis and morphological alterations of A375 cells. After 72 h treatment of cells with 50 μM FC, TMZ 400 μM and their combination, apoptosis was detected using annexin V-FITC and PI staining followed by flow cytometry (A). Cells were classified as viable (negative for both annexin V-FITC and PI), necrotic (PI-positive only), or apoptotic—early or late (annexin V-FITC positive). Phase-contrast images illustrate changes in cell density and morphology in A375 cells after 72 h combined treatment with 50 μM FC and 400 μM TMZ (B).

observations supported the viability and flow cytometry results, showing a reduced number of attached and viable A375 cells after 72 h of combined treatment with 50 μM FC and 400 μM TMZ compared to controls (Figure 8B).

4. Discussion

Melanoma continues to surge globally, with developed nations witnessing a particularly alarming rise in cases[40]. While early-stage melanoma is often curable through surgery, advanced metastatic disease poses a formidable challenge, demanding aggressive interventions such as immunotherapy, targeted therapy, radiotherapy, or chemotherapy. Current treatments, however, face critical limitations. Chemotherapeutics like TMZ suffer from short half-lives, necessitating high doses that trigger severe side effects and drug resistance[7]. Meanwhile, cutting-edge options like immunotherapy and targeted therapies remain prohibitively expensive and inaccessible for many patients. These hurdles underscore an urgent need for safer, affordable, and effective alternatives, ideally derived from natural sources with inherent biocompatibility. In the present study, we pioneer the first investigation into whether FC—a natural sesquiterpene coumarin—can enhance chemotherapy and IR efficacy against human melanoma cells, aiming to bridge critical therapeutic gaps by synergizing with conventional treatments.

TOP2 is a vital enzyme responsible for maintaining genomic integrity by managing the compact folding of large DNA molecules within the nucleus during transcription and replication[41,42]. TOP2A expression increases during the S phase and peaks at the G_2/M phase in rapidly dividing cells, whereas TOP2B expression remains stable and low[43,44]. TOP2A is a key target in anticancer drug development, with approximately 50% of antitumor drugs acting as topoisomerase inhibitors[45]. Assessment of *TOP2A* expression confirmed its marked upregulation in melanoma, both at the tissue level and in A375 cells. Additionally, elevated *TOP2A* expression in SKCM was found to correlate with poorer patient survival, highlighting its prognostic significance and supporting findings from previous studies[14,15,20].

To investigate whether FC has the potential to inhibit TOP2A enzymatic activity, molecular docking and dynamics simulations were conducted, providing a comprehensive characterisation of FC binding interactions. These analyses demonstrated stable, high-affinity engagement with TOP2A, involving critical ATP-binding site residues Ser148, Ser149, and Lys168, which are essential for enzymatic function[16,46]. FC exhibited docking affinity superior to that of the established inhibitor Etoposide, highlighting a strong and specific capacity to target TOP2A and positioning FC as a promising therapeutic candidate for melanoma treatment. To experimentally evaluate the potential of FC as a TOP2A inhibitor that enhances the

DNA-damaging effects of radiotherapy and the alkylating agent TMZ, human melanoma cells and normal fibroblasts were treated with FC alone or in combination with IR or TMZ, and assessed for viability and apoptosis. SI values calculated from the viability assay confirmed the selective cytotoxicity of FC towards melanoma cells. Combination treatments of FC with IR or TMZ significantly potentiated their effects, markedly increasing apoptotic cell death. This enhancement is likely driven by FC-mediated inhibition of TOP2A, impairing DNA repair mechanisms that resolve IR- and TMZ-induced double-strand breaks. Consequently, the interference of FC with TOP2A-dependent DNA topology modulation hampers the repair of DNA lesions caused by these treatments, thereby amplifying cell death. These findings support the role of FC as a TOP2A inhibitor and suggest its promise as a sensitising agent in melanoma therapy.

These results are consistent with previous studies reporting that FC induced apoptosis and G_1-phase arrest in various cancer cell lines—including HepG2, K562, MCF-7, and NSCLC cells—through activation of caspase-3 and regulation of key effectors such as BAX/BCL-2, Cyclin D1, and P21[25,26,29,47]. Moreover, FC has been shown to reverse multidrug resistance in breast cancer cell lines[30,48] and sensitise leukaemia cells to Imatinib via caspase activation and histone deacetylase inhibition[26]. Combined treatment of lung carcinoma cells with FC and chemotherapeutic agents such as Puromycin or Doxorubicin further enhanced caspase activation and suppressed cell cycle regulators more effectively than monotherapies[24,27,30,48].

The present study focused on evaluating the effects of FC in combination therapy on human melanoma cell viability and apoptosis, alongside analyses of the interaction between FC and TOP2A. While these findings are promising, further investigation at the protein level, including assessment of apoptosis-related factors such as caspases, Bax, and Bcl-2, is recommended. Future research should also validate the effects of FC across a wider range of melanoma cell lines and explore its potential synergy with other chemotherapeutic agents. Addressing these aspects will provide a more comprehensive understanding of the apoptotic mechanisms involved and better define the therapeutic potential of FC in combination treatments.

5. Conclusion

The present study reports for the first time the effects of FC in combination with radiation and chemotherapy on melanoma cells through interaction with TOP2A, which exhibits elevated expression in melanoma. These findings open new avenues for therapeutic strategy development and provide a strong rationale for further preclinical and clinical evaluation of FC, as well as other natural sesquiterpene coumarins.

Authors' contributions

CRediT: **Negin Moosavinejad**: Formal analysis, Investigation, Writing – original draft; **Zahra Nasiri Sarvi**: Formal analysis; **Hamid Gholamhosseinian**: Methodology, Resources; **Mehrdad Iranshahi**: Methodology, Resources; **Fatemeh B. Rassouli**: Conceptualization, Supervision, Writing – review & editing.

Disclosure statement

No potential conflict of interest was reported by the author(s).

Availability of data and materials

The data that support the findings of this study are available from the corresponding author upon reasonable request.

References

1. Lopes J, Rodrigues CM, Gaspar MM, Reis CP. Melanoma management: from epidemiology to treatment and latest advances. Cancers (Basel). 2022;14(19):4652.
2. Garbe C, Amaral T, Peris K, Hauschild A, Arenberger P, Basset-Seguin N, Bastholt L, Bataille V, Del Marmol V, Dréno B, European Association of Dermato-Oncology (EADO, et al. European consensus-based interdisciplinary guideline for melanoma. Part 2: treatment-update 2022. Eur J Cancer. 2022;170:256–284.
3. Goldinger SM, Buder-Bakhaya K, Lo SN, Forschner A, McKean M, Zimmer L, Khoo C, Dummer R, Eroglu Z, Buchbinder EI, et al. Chemotherapy after immune checkpoint inhibitor failure in metastatic melanoma: a retrospective multicentre analysis. Eur J Cancer. 2022;162:22–33.
4. Dabestani PJ, Dawson AJ, Neumeister MW, Bradbury CM. Radiation therapy for local cutaneous melanoma. Clin Plast Surg. 2021;48(4):643–649.
5. Davis LE, Shalin SC, Tackett AJ. Current state of melanoma diagnosis and treatment. Cancer Biol Ther. 2019;20(11):1366–1379.
6. Atkins MB, Lee SJ, Chmielowski B, Tarhini AA, Cohen GI, Truong T-G, Moon HH, Davar D, O'Rourke M, Stephenson JJ, et al. Combination dabrafenib and trametinib versus combination nivolumab and ipilimumab for patients with advanced BRAF-mutant melanoma: the DREAMseq trial—ECOG-ACRIN EA6134. J Clin Oncol. 2023;41(2):186–197.
7. Trinh VA, Patel SP, Hwu WJ. The safety of temozolomide in the treatment of malignancies. Expert Opin Drug Saf. 2009;8(4):493–499.
8. Zhao S, Sun W, Sun J, Peng L, Wang C. Clinical features, treatment, and outcomes of nivolumab induced psoriasis. Invest New Drugs. 2025;43(1):42–49.
9. Wu Z, Li X, Huang R, He B, Wang C. Clinical features, treatment, and prognosis of pembrolizumab-induced Stevens-Johnson syndrome/toxic epidermal necrolysis. Invest New Drugs. 2025;43(1):74–80.
10. Gelsleichter NE, de Souza PO, Teixeira FC, Debom GN, Lenz GS, Roliano GG, de Cássia Sant'ana R, Visioli F, Fachel FNS, Michels LR, et al. Metastatic melanoma: a preclinical model standardization and development of a chitosan-coated nanoemulsion containing temozolomide to treat brain metastasis. Cell Mol Neurobiol. 2023;43(6):2939–2951.
11. Sun W, Jang M-S, Zhan S, Liu C, Sheng L, Lee JH, Fu Y, Yang HY. Tumor-targeting and redox-responsive photo-cross-linked nanogel derived from multifunctional hyaluronic acid-lipoic acid conjugates for enhanced in vivo protein delivery. Int J Biol Macromol. 2025;314:144444.
12. Jiang Z, Chen Z, Xu Y, Li H, Li Y, Peng L, Shan H, Liu X, Wu H, Wu L, et al. Low-frequency ultrasound sensitive Piezo1 channels regulate keloid-related characteristics of fibroblasts. Adv Sci. 2024;11(14):2305489.
13. Chen Y, Deng Y, Li Y, Qin Y, Zhou Z, Yang H, Sun Y. Oxygen-independent radiodynamic therapy: radiation-boosted chemodynamics for reprogramming the tumor immune environment and enhancing antitumor immune response. ACS Appl Mater Interfaces. 2024;16(17):21546–21556.
14. Skok Ž, Durcik M, Zajec Ž, Gramec Skledar D, Bozovičar K, Pišlar A, Tomašič T, Zega A, Peterlin Mašič L, Kikelj D, et al. ATP-competitive inhibitors of human DNA topoisomerase IIα with improved antiproliferative activity based on N-phenylpyrrolamide scaffold. Eur J Med Chem. 2023;249:115116.
15. McKie SJ, Neuman KC, Maxwell A. DNA topoisomerases: Advances in understanding of cellular roles and multi-protein complexes via structure-function analysis. Bioessays. 2021;43(4):e2000286.
16. Bergant Loboda K, Janežič M, Štampar M, Žegura B, Filipič M, Perdih A. Substituted 4, 5′-bithiazoles as catalytic inhibitors of human DNA topoisomerase IIα. J Chem Inf Model. 2020;60(7):3662–3678.
17. Wendorff TJ, Schmidt BH, Heslop P, Austin CA, Berger JM. The structure of DNA-bound human topoisomerase II alpha: conformational mechanisms for coordinating inter-subunit interactions with DNA cleavage. J Mol Biol. 2012;424(3-4):109–124.
18. Lindsey RH, Jr, Pendleton M, Ashley RE, Mercer SL, Deweese JE, Osheroff N. Catalytic core of human topoisomerase IIα: insights into enzyme–DNA interactions and drug mechanism. Biochemistry. 2014;53(41):6595–6602.
19. Pogorelčnik B, Perdih A, Solmajer T. Recent developments of DNA poisons-human DNA topoisomerase IIα inhibitors-as anticancer agents. Curr Pharm Des. 2013;19(13):2474–2488.
20. Okoro CO, Fatoki TH. A mini review of novel topoisomerase ii inhibitors as future anticancer agents. Int J Mol Sci. 2023;24(3):2532.
21. Valiahdi SM, Iranshahi M, Sahebkar A. Cytotoxic activities of phytochemicals from Ferula species. Daru. 2013;21(1):39.
22. Zhou Y, Xin F, Zhang G, Qu H, Yang D, Han X. Recent advances on bioactive constituents in Ferula. Drug Dev Res. 2017;78(7):321–331.
23. Sistani P, Dehghan G, Sadeghi L. Structural and kinetic insights into HIV-1 reverse transcriptase inhibition by farnesiferol C. Int J Biol Macromol. 2021;174:309–318.
24. Chang HJ, Kim YS, Ryu SY, Chun HS. Screening of various sources of phytochemicals for neuroprotective activity against oxygen-glucose deprivation in vitro. J Korean Soc Appl Biol Chem. 2013;56(4):451–455.
25. Alafnan A, Alamri A, Alanazi J, Hussain T. Farnesiferol C exerts Antiproliferative effects on hepatocellular carcinoma HepG2 cells by instigating ROS-dependent apoptotic pathway. Pharmaceuticals. 2022;15(9):1070.

26. Jung JH, Park JE, Sim DY, Im E, Park WY, Lee D, Shim B-S, Kim S-H. Farnesiferol C induces apoptosis in chronic myelogenous leukemia cells as an imatinib sensitizer via caspase activation and HDAC (histone deacetylase) inactivation. Int J Mol Sci. 2019;20(22):5535.

27. Tanzadehpanah H, Mahaki H, Samadi P, Karimi J, Moghadam NH, Salehzadeh S, Dastan D, Saidijam M. Anticancer activity, calf thymus DNA and human serum albumin binding properties of Farnesiferol C from Ferula pseudal-liacea. J Biomol Struct Dyn. 2019;37(11):2789–2800.

28. Aldaghi L, Rad A, Arab A, Kasaian J, Iranshahi M, Sadr AS, Soltani F. In silico and in vitro evaluation of cytotoxic activities of farnesiferol c and microlobin on MCF-7, HeLa and KYSE cell lines. Drug Res (Stuttg). 2016;66(10):532–538.

29. Jung JH, Kim MJ, Lee H, Lee J, Kim J, Lee HJ, Shin EA, Kim YH, Kim B, Shim BS, et al. Farnesiferol c induces apoptosis via regulation of L11 and c-Myc with combinational potential with anticancer drugs in non-small-cell lung cancers. Sci Rep. 2016;6(1):26844.

30. Kasaian J, Mosaffa F, Behravan J, Masullo M, Piacente S, Ghandadi M, Iranshahi M. Reversal of P-glycoprotein-mediated multidrug resistance in MCF-7/Adr cancer cells by sesquiterpene coumarins. Fitoterapia. 2015;103:149–154.

31. Buniello A, Suveges D, Cruz-Castillo C, Llinares MB, Cornu H, Lopez I, Tsukanov K, Roldán-Romero JM, Mehta C, Fumis L, et al. Open Targets Platform: facilitating therapeutic hypotheses building in drug discovery. Nucleic Acids Res. 2025;53(D1):D1467–D1475.

32. Daina A, Michielin O, Zoete V. SwissTargetPrediction: updated data and new features for efficient prediction of protein targets of small molecules. Nucleic Acids Res. 2019;47(W1):W357–W364.

33. Szklarczyk D, Kirsch R, Koutrouli M, Nastou K, Mehryary F, Hachilif R, Gable AL, Fang T, Doncheva NT, Pyysalo S, et al. The STRING database in 2023: protein–protein association networks and functional enrichment analyses for any sequenced genome of interest. Nucleic Acids Res. 2023;51(D1):D638–D646.

34. Bartha Á, Győrffy B. TNMplot. com: a web tool for the comparison of gene expression in normal, tumor and metastatic tissues. Int J Mol Sci. 2021;22(5):2622.

35. Tang Z, Kang B, Li C, Chen T, Zhang Z. GEPIA2: an enhanced web server for large-scale expression profiling and interactive analysis. Nucleic Acids Res. 2019;47(W1):W556–W560.

36. Schöning-Stierand K, Diedrich K, Ehrt C, Flachsenberg F, Graef J, Sieg J, Penner P, Poppinga M, Ungethüm A, Rarey M. ProteinsPlus: a comprehensive collection of web-based molecular modeling tools. Nucleic Acids Res. 2022;50(W1):W611–w615.

37. Diedrich K, Krause B, Berg O, Rarey M. PoseEdit: enhanced ligand binding mode communication by interactive 2D diagrams. J Comput Aided Mol Des. 2023;37(10):491–503.

38. Flachsenberg F, Meyder A, Sommer K, Penner P, Rarey M. A Consistent Scheme for Gradient-Based Optimization of Protein–Ligand Poses. J Chem Inf Model. 2020;60(12):6502–6522.

39. Iranshahi M, Arfa P, Ramezani M, Jaafari MR, Sadeghian H, Bassarello C, Piacente S, Pizza C. Sesquiterpene coumarins from Ferula szowitsiana and in vitro antileishmanial activity of 7-prenyloxycoumarins against promasti-gotes. Phytochemistry. 2007;68(4):554–561.

40. Arnold M, Singh D, Laversanne M, Vignat J, Vaccarella S, Meheus F, Cust AE, de Vries E, Whiteman DC, Bray F. Global burden of cutaneous melanoma in 2020 and projections to 2040. JAMA Dermatol. 2022;158(5):495–503.

41. Noy A, Sutthibutpong T, SA, Harris Protein/DNA interactions in complex DNA topologies: expect the unexpected. Biophys Rev. 2016;8(Suppl 1):145–155.

42. Pommier Y, Sun Y, Huang SYN, Nitiss JL. Roles of eukaryotic topoisomerases in transcription, replication and genomic stability. Nat Rev Mol Cell Biol. 2016;17(11):703–721.

43. McClendon AK, Osheroff N. DNA topoisomerase II, genotoxicity, and cancer. Mutat Res. 2007;623(1-2):83–97.

44. Baviskar AT, Madaan C, Preet R, Mohapatra P, Jain V, Agarwal A, Guchhait SK, Kundu CN, Banerjee UC, Bharatam PV. N-fused imidazoles as novel anticancer agents that inhibit catalytic activity of topoisomerase IIα and induce apoptosis in G1/S phase. J Med Chem. 2011;54(14):5013–5030.

45. Nitiss JL. DNA topoisomerase II and its growing repertoire of biological functions. Nat Rev Cancer. 2009;9(5):327–337.

46. Wei H, Ruthenburg AJ, Bechis SK, Verdine GL. Nucleotide-dependent domain movement in the ATPase domain of a human type IIA DNA topoisomerase. J Biol Chem. 2005;280(44):37041–37047.

47. Hasanzadeh D, Mahdavi M, Dehghan G, Charoudeh HN. Farnesiferol C induces cell cycle arrest and apoptosis mediated by oxidative stress in MCF-7 cell line. Toxicol Rep. 2017;4:420–426.

48. Kasaian J, Mosaffa F, Behravan J, Masullo M, Piacente S, Iranshahi M. Modulation of multidrug resistance protein 2 efflux in the cisplatin resistance human ovarian carcinoma cells A2780/RCIS by sesquiterpene coumarins. Phytother Res. 2016;30(1):84–89.